Supporting Information

From cotton to functional flexible transparent film for printable and flexible micro-supercapacitor with strong bonding interface

Wenjie Zhang,*[a] Bohan Li,[b] Ruitao Lv,[b] Huaming Li,[a] Yuqing Weng,[b] Wanci Shen,[b] Feiyu Kang[b] and Zheng-Hong Huang*[bc]

[a] *Institute for Energy Research, Jiangsu University, Zhenjiang 212013, China, E-mail:*
 zwenjie@ujs.edu.cn; zwenjie1008@hotmail.com.

[b] *State Key Laboratory of New Ceramics and Fine Processing, School of Materials Science and Engineering, Tsinghua University, Beijing 100084, China, E-mail: zhhuang@mail.tsinghua.edu.cn*

[c] *Key Laboratory of Advanced Materials (MOE), School of Materials Science and Engineering, Tsinghua University, Beijing 100084, China*

1. Experimental section

Synthesis of functional flexible transparent film

Briefly, 12 g cotton was dispersed in 700 ml deionized water with an agitator. Then, 20 ml 1 wt% 2,2,6,6-tetramethylpiperidin-1-oxyl (TEMPO) aqueous solution and 20 ml 10 wt% NaBr aqueous solution were added to the cotton suspension. After stirring uniformly, 100 g NaClO (Cl conc. 8 %) was slowly added in the above mixture solution. During this process, 3 M NaOH solution was used to adjust and maintain the PH of the mixture solution around 10.5. After the reaction, the oxidized cotton fibers were washed 3 times with deionized water. And then, mechanical shearing was applied to the oxidized cotton fibers. Lastly, the obtained nanometer-scale cotton fibers were assembled into functional flexible transparent film through vacuum filtration.

Inkjet Printing text, QR-code

The texts and QR-code were directly inkjet-printed on the functional flexible transparent film with an inkjet printer (EPSON, L4268).

Preparation of gel electrolyte PVDF-HFP/LiTFSI

PVDF-HFP was dissolved in acetone by magnetically stirring at 60 °C. Then, LiTFSI was added to the above PVDF-HFP/acetone solution. Here, the mass ratio of LiTFSI to PVDF-HFP is 9. The resulting mixture was stirred for 3 h at room temperature to yield

a homogenous solution. Lastly, the solution was casted onto the micro-supercapacitor and dried naturally overnight to formed the gel electrolyte PVDF-HFP/LiTFSI.

Fabrication of micro-supercapacitor on film

The flexible micro-supercapacitor was constructed on the functional transparent film through mask-assisted filtration of the rGO/CNT solution. Here, the mass ratio of rGO to CNT is 9. After removing water from rGO/CNT solution by vacuum filtration, the rGO/CNT deposited on transparent film to form the interdigitated micro-supercapacitor.

Material Characterizations

The morphology and structure of samples were examined by scanning electron microscopy (SEM, JSM-7001F, JEOL) and transmission electron microscopy (TEM, JEM-2100F, JEOL). The surface modification was characterized using Fourier transform infrared spectra (FTIR, Bruker Vector-22). The transmittance was measured by UV-vis spectrophotometer (UV-vis, UV-2450).

Electrochemical Measurements

The electrochemical performances were obtained on an electrochemical workstation (VMP3, Bio-Logic). CV curves were tested in the potential range of 0-3.5 V at scan rates from 5 to 200 mV s^{-1}. GCD profiles were obtained at current densities of 0.5 to 1.4 mA cm^{-2}. EIS curve was measured in the frequency range from 0.01 Hz to 100 kHz with AC amplitude 10 mV.

2. Calculation

The areal capacitance (C) calculated from the GCD curves is obtained by using the formula:

$$C = \frac{I\Delta t}{A\Delta U} \qquad (1)$$

Where I is the constant discharge current, Δt is the discharge time, A is the total area of the electrodes, ΔU is the voltage window after excluding the Ohmic drop (IR).

The volumetric energy density E and power density P derived from the GCD curves are calculated from formula (2) and (3):

$$E = \frac{1}{2} \times C \times \frac{\Delta U^2}{3600}$$ (2)

$$P = \frac{E}{\Delta t} \times 3600$$ (3)

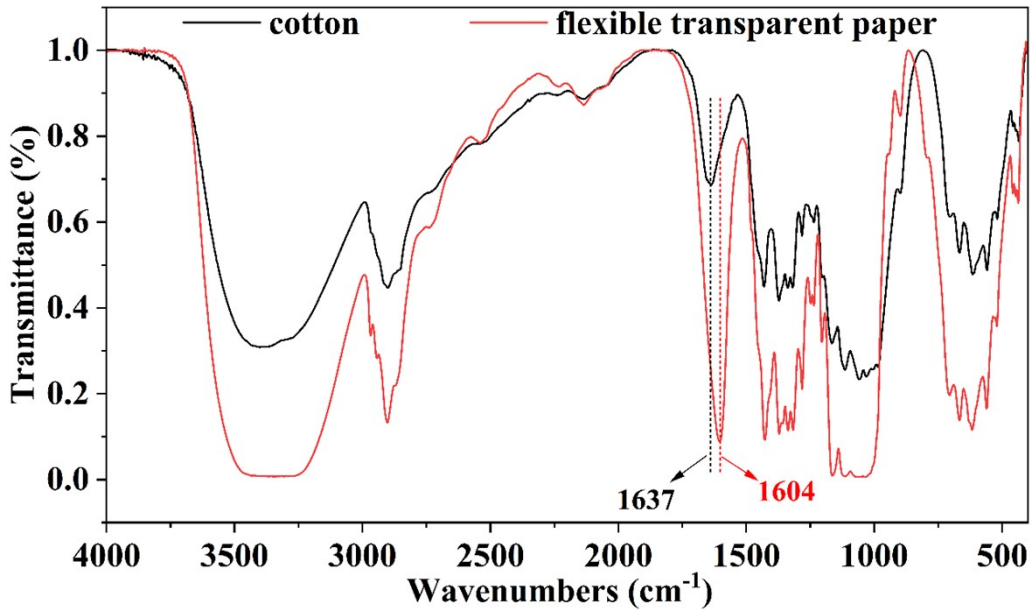## 3. Figures and discussion

Fig. S1 FTIR spectra of the raw cotton and the obtained flexible transparent paper.

Fig. S1 shows the Fourier transform infrared (FTIR) spectra of the cotton fibers before and after TEMPO and mechanical shearing treatments. All the spectrums show a broad peak from 3200 to 3500 cm^{-1}, which are associated with O-H stretching vibration.[1-3] For raw cotton, the peak at 1637 cm^{-1} is related to the C=O stretching (amide II) from non-cellulosic components consisting of wax, protein and pectin at the cotton fiber surface.[1, 4, 5] The peak disappears in the cotton nanocellulose, which indicates the removal of non-cellulosic components from the cotton fiber surface after chemical treatment. For the cotton nanocellulose, a strong peak at 1604 cm^{-1} derived from the carbonyl groups appears, confirming that C6-primary hydroxyl groups of cotton cellulose chains are converted to C6-carboxyl groups via TEMPO-mediated oxidation.[6, 7]
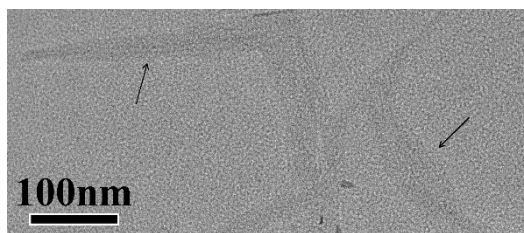
Fig. S2 High magnification TEM image of nanometer-scale cotton cellulose fibers.

Fig. S2 shows the high magnification TEM image of the nanometer-scale cotton cellulose fibers. It displays that the exfoliated cotton cellulose fibers have a fine size and ribbon-like structure.
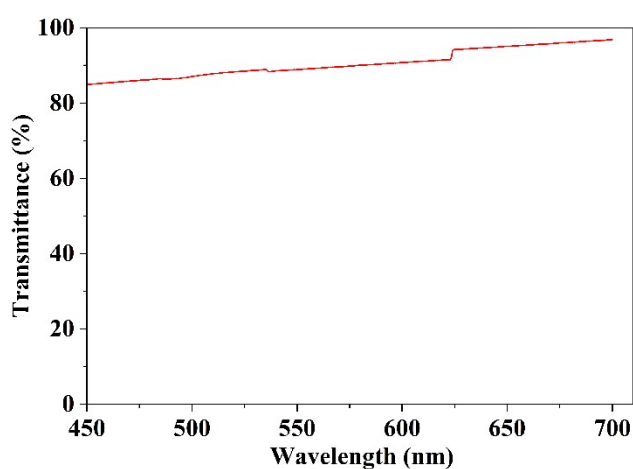

Fig. S3 Transmittance of the functional flexible transparent film.
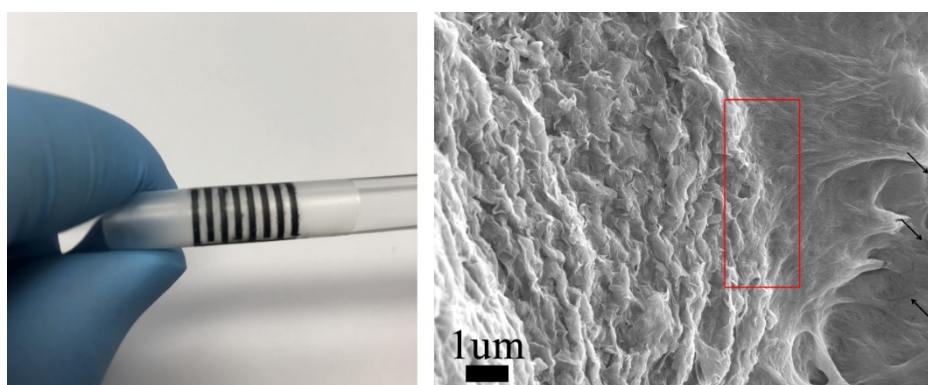

Fig. S4 (a) Photograph of the deformation of the flexible micro-supercapacitor. (b) Morphology of the flexible micro-supercapacitor after 150 bending deformations.

Fig. S4 shows the morphology of the flexible micro-supercapacitor after 150 times wrapping around a glass rod. At the high magnification, only several microcracks are observed in electrode materials in the marginal region, marked by the arrow in Fig. S4b.

However, the electrode materials are still tightly attached to the transparent film without shedding, marked by red square in Fig. S4b. The binder-free flexible micro-supercapacitor maintains structural stability well after so many large deformations, demonstrating the superior interfacial adhesion and reliability of the cotton-derived flexible transparent film in the wearable device manufacturing.
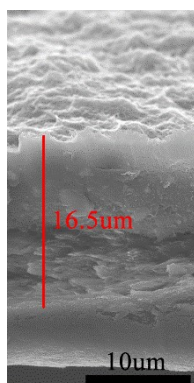

Fig. S5 Cross-section image of the flexible micro-supercapacitor.
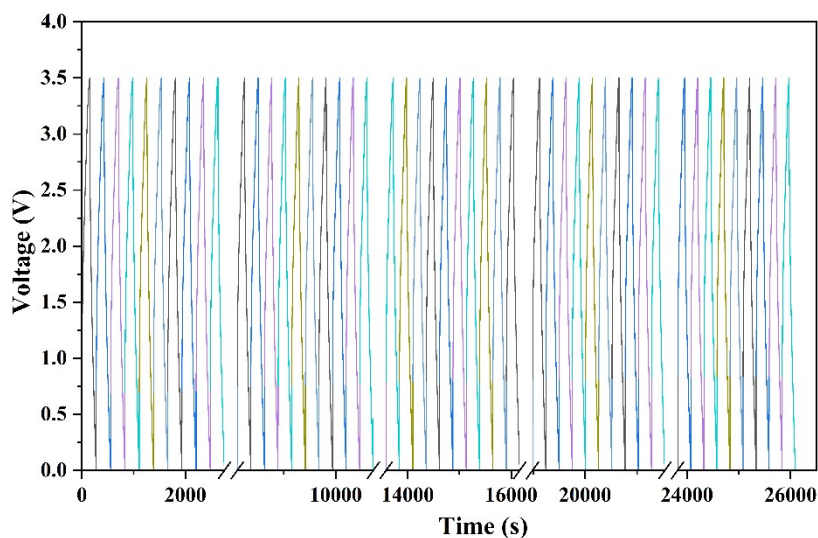

Fig. S6 Cycle stability of the flexible micro-supercapacitor at 0.7 mA cm^{-2}.

The capacitance retention of the flexible micro-supercapacitor over bending times was investigated, as shown in Fig. S7. The bending is carried out by wrapping the micro-supercapacitor around a glass rod, as shown in Fig. S4a. The flexible micro-supercapacitor exhibits a high capacitance retention of 87 % and 81.5 % after 100 and 150 bending times, respectively. The results also indicate the applicability of the cotton-derived functional flexible transparent film to flexible micro-supercapacitor and
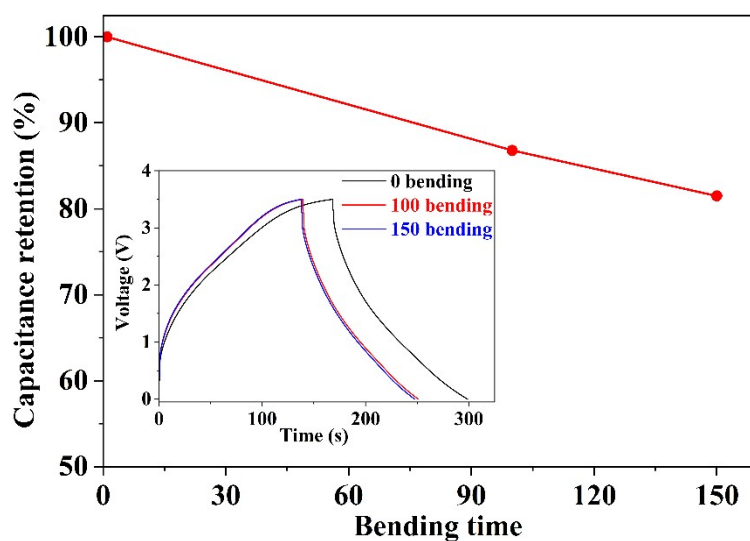
wearable devices.

Fig. S7 Capacitance retention of the flexible micro-supercapacitor versus bending times at 0.7 mA cm^{-2}, inset is GCD curves for different bending times.

Table S1 Performance comparison of graphene-based micro-supercapacitor fabricated on various substrates.

Electrode	Substrate	C (mF cm^{-2})	Refs.
rGO/CNT	functional flexible transparent film	39.1@0.5 mA cm^{-2}	This work
graphene -boron doped diamond nanowall	PI	9.4@0.1 mA cm^{-2}	[8]
graphene	PI	3.9@0.2 mA cm^{-2}	[9]
TiO$_2$-graphene	PET	9.9@5 uA/cm^{-2}	[10]
KOH-activated 3D graphene	PI	32@0.05 mA cm^{-2}	[11]
3D porous graphene/ phosphorene	PI	16.94@0.2 mA/cm^{-2}	[12]
boron-doped laser-induced graphene	PI	16.5@0.05mA/cm^{-2}	[13]

fluorine-modified graphene	PET	17.4@1 mV s^{-1}	[14]
electrochemically exfoliated graphene	PET	2@5 mV s^{-1}	[15]
rGO/RuO$_2$	PET	2.35@20 mV s^{-1}	[16]
Laser-induced graphene	PI	0.62 @ 5 mV s^{-1}	[17]
graphene-phosphorene	PET	9.8 @ 5 mV s^{-1}	[18]

References

1 S. Yang, L. Chen, S. Liu, W. Hou, J. Zhu, P. Zhao and Q. Zhang, *J. Hazard. Mater.*, 2021, **408**, 124408.

2 Z. Ling, T. Wang, M. Makarem, M. Santiago Cintrón, H. Cheng, X. Kang, M. Bacher, A. Potthast, T. Rosenau and H. King, *Cellulose*, 2019, **26**, 305-328.

3 M. M. Mahmud, A. Perveen, R. A. Jahan, M. A. Matin, S. Y. Wong, X. Li and M. T. Arafat, *Int. J. Biol. Macromol.*, 2019, **130**, 969-976.

4 R. Mitchell, C. M. Carr, M. Parfitt, J. Vickerman and C. Jones, *Cellulose*, 2005, **12**, 629-639.

5 L. Zhang, X. Li, S. Zhang, Q. Gao, Q. Lu, R. Peng, P. Xu, H. Shang, Y. Yuan and H. Zou, *Anal. Bioanal. Chem.*, 2021, **413**, 1313-1320.

6 D. Marković, M. Korica, M. Kostić, Ž. Radovanović, Z. Šaponjić, M. Mitrić and M. Radetić, *Cellulose*, 2018, **25**, 829-841.

7 S. Ifuku, M. Tsuji, M. Morimoto, H. Saimoto and H. Yano, *Biomacromolecules*, 2009, **10**, 2714-2717.

8 S. Deshmukh, P. Jakobczyk, M. Ficek, J. Ryl, D. Geng and R. Bogdanowicz, *Adv. Funct. Mater.*, 2022, **32**, 2206097.

9 J. Lin, Z. Peng, Y. Liu, F. Ruiz-Zepeda, R. Ye, E. L. Samuel, M. J. Yacaman, B. I. Yakobson and J. M. Tour, *Nat. Commun.*, 2014, **5**, 1-8.

10 L. Fornasini, S. Scaravonati, G. Magnani, A. Morenghi, M. Sidoli, D. Bersani, G. Bertoni, L. Aversa, R. Verucchi and M. Riccò, *Carbon*, 2021, **176**, 296-306.

11 H. Liu, Y. Xie, J. Liu, K.-s. Moon, L. Lu, Z. Lin, W. Yuan, C. Shen, X. Zang and L. Lin, *Chem. Eng. J.*, 2020, **393**, 124672.

12 M. A. Zahed, S. C. Barman, M. Sharifuzzaman, S. Zhang, H. Yoon, C. Park, S. H. Yoon and J. Y. Park, *Adv. Funct. Mater.*, 2021, **31**, 2009018.

13 Z. Peng, R. Ye, J. A. Mann, D. Zakhidov, Y. Li, P. R. Smalley, J. Lin and J. M. Tour, *ACS Nano*, 2015, **9**, 5868-5875.

14 F. Zhou, H. Huang, C. Xiao, S. Zheng, X. Shi, J. Qin, Q. Fu, X. Bao, X. Feng and K. Müllen, *J. Am. Chem. Soc.*, 2018, **140**, 8198-8205.

15 Z. Liu, Z. S. Wu, S. Yang, R. Dong, X. Feng and K. Müllen, *Adv. Mater.*, 2016, **28**, 2217-2222.

16 L. Wang, Y. Ding, J. Li, Y. Guan, L. Yang, H. Fang, X. Lv and J. Yuan, *J. Electroanal. Chem.*, 2022, 116501.

17 X. Shi, F. Zhou, J. Peng, R. a. Wu, Z. S. Wu and X. Bao, *Adv. Funct. Mater.*, 2019, **29**, 1902860.

18 H. Xiao, Z.-S. Wu, L. Chen, F. Zhou, S. Zheng, W. Ren, H.-M. Cheng and X. Bao, *ACS Nano*, 2017, **11**, 7284-7292.